


Discovering QCD-coupled axion dark matter with polarization haloscopes

Asher Berlin^{1,2,*} and Kevin Zhou^{3,†}

¹Theory Division, Fermi National Accelerator Laboratory, Batavia, Illinois 60510, USA

²Superconducting Quantum Materials and Systems Center (SQMS),
Fermi National Accelerator Laboratory, Batavia, Illinois 60510, USA

³SLAC National Accelerator Laboratory, 2575 Sand Hill Road, Menlo Park, California 94025, USA

 (Received 3 October 2022; revised 24 March 2023; accepted 31 July 2023; published 25 August 2023)

In the presence of QCD axion dark matter, atoms acquire time-dependent electric dipole moments. This effect gives rise to an oscillating current in a nuclear spin-polarized dielectric, which can resonantly excite an electromagnetic mode of a microwave cavity. We show that with existing technology such a “polarization haloscope” can explore orders of magnitude of new parameter space for QCD-coupled axions. If any cavity haloscope detects a signal from the axion-photon coupling, an upgraded polarization haloscope has the unique ability to test whether it arises from the QCD axion.

DOI: [10.1103/PhysRevD.108.035038](https://doi.org/10.1103/PhysRevD.108.035038)

I. INTRODUCTION

The QCD axion is a long-standing, well-motivated dark matter candidate [1–7] that can also explain why the neutron’s electric dipole moment (EDM) is at least 10^{10} times smaller than generically expected [8]. It is a pseudoscalar field a defined by its coupling to gluons,

$$\mathcal{L} \supset \theta_a \frac{\alpha_s}{8\pi} G^{\mu\nu} \tilde{G}_{\mu\nu}, \quad (1)$$

where $\theta_a \equiv a/f_a$ and f_a is the axion decay constant. At temperatures below the QCD phase transition, this coupling generates a potential and mass for the axion [9],

$$m_a = 5.7 \mu\text{eV} \times (10^{12} \text{ GeV}/f_a). \quad (2)$$

Over cosmological time, the axion field relaxes towards the minimum of its potential at the parity (\mathcal{P}) and time-reversal (\mathcal{T}) conserving point $\theta_a = 0$ where the neutron EDM vanishes. Assuming a standard cosmological history and an $\mathcal{O}(1)$ initial misalignment angle, the residual energy in the axion field accounts for the present density of cold dark matter for $m_a \sim (0.5\text{--}50) \mu\text{eV}$ [10]. In this case, the local axion field has macroscopic mode occupancy and can thus be described by a classical expectation value,

$$\theta_a \simeq \frac{\sqrt{2\rho_{\text{DM}}}}{m_a f_a} \cos m_a t \simeq 4.3 \times 10^{-19} \cos m_a t, \quad (3)$$

oscillating with frequency $m_a/2\pi \sim (0.1\text{--}10)$ GHz, where $\rho_{\text{DM}} \simeq 0.4 \text{ GeV}/\text{cm}^3$ is the local dark matter density.

The direct signatures of QCD axion dark matter are nuclear effects, such as the oscillating neutron EDM [11],

$$d_n \simeq (2.4 \times 10^{-3} e \text{ fm}) \theta_a. \quad (4)$$

Detecting such a small signal is very difficult, but has been addressed by several recent proposals. In some cases, static EDM experiments may be repurposed to constrain slowly oscillating EDMs [12–14]. Other potential detection avenues involve nuclear magnetic resonance [15–17], spin precession in storage rings [18–23], atomic and molecular spectroscopy [24,25], and mechanical oscillations in piezoelectric materials [26]. However, none of these probes are sensitive at the GHz frequencies motivated by standard misalignment production of axion dark matter.

Currently, the most stringent laboratory constraints on axion dark matter at GHz frequencies come from cavity haloscopes [27,28], which rely on the axion’s coupling to photons, $\mathcal{L} \supset g_{a\gamma\gamma} a F^{\mu\nu} \tilde{F}_{\mu\nu}/4$. In these experiments, axion dark matter produces an effective current $\mathbf{J}_{a\gamma\gamma} = g_{a\gamma\gamma} \mathbf{B} \partial_t a$ inside a microwave cavity with background magnetic field \mathbf{B} , which can resonantly excite a mode of angular frequency m_a . While there are many other recent proposals to search for the axion (see Refs. [29–31] for reviews), the cavity haloscope concept is currently the most well developed, with many collaborations reporting new results [32–50] and some operating near or beyond the standard quantum limit [34,36,37,42]. These experiments are well motivated, as the axion-gluon coupling of Eq. (1) is known

*aberlin@fnal.gov

†knzhou@stanford.edu

Published by the American Physical Society under the terms of the [Creative Commons Attribution 4.0 International license](https://creativecommons.org/licenses/by/4.0/). Further distribution of this work must maintain attribution to the author(s) and the published article’s title, journal citation, and DOI. Funded by SCOAP³.

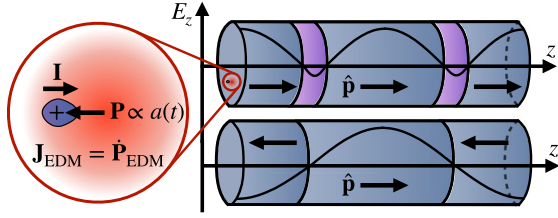


FIG. 1. Atoms carry EDMs proportional to the axion field (left), aligned with the nuclear spin \mathbf{I} . The axion's time variation thus produces a current \mathbf{J}_{EDM} in a nuclear spin-polarized dielectric, whose effect can be amplified in a resonant cavity. For higher axion masses, the geometric overlap factor in Eq. (19) can be maximized using layers of inert dielectric (top) or alternating spin polarization (bottom).

to induce an axion-photon coupling. However, their relation is indirect: the coefficient $g_{a\gamma\gamma}$ can vary by orders of magnitude within simple models [51–54], and an axion with an electromagnetic coupling is not necessarily the QCD axion. Definitively discovering or excluding the QCD axion thus requires confronting the axion-gluon coupling directly.

In this work, we present the first method to probe the axion-gluon coupling at GHz frequencies. In the presence of axion dark matter, atoms have oscillating EDMs of magnitude d_A directed along their nuclear spin [55], analogous to the neutron EDM in Eq. (4). A dielectric thus carries a polarization density $P_{\text{EDM}} \sim n_A d_A$, where n_A is the density of nuclear spin-polarized atoms. A time-varying polarization induces a physical electromagnetic current $\mathbf{J}_{\text{EDM}} = \partial_t \mathbf{P}_{\text{EDM}}$, which can be resonantly amplified by placing the dielectric in a microwave cavity with a mode of angular frequency m_a . We call this system, depicted in Fig. 1, a polarization haloscope.

To quickly estimate its potential, we may compare the current in a polarization haloscope to that produced in a typical cavity haloscope. For the benchmark DFSZ model, where $g_{a\gamma\gamma} \simeq 0.87 \times 10^{-3}/f_a$ [56,57], the ratio is

$$\frac{J_{\text{EDM}}}{J_{a\gamma\gamma}} \simeq 10^{-3} \times \frac{d_A}{d_n} \left(\frac{n_A}{5 \times 10^{22} \text{ cm}^{-3}} \right) \left(\frac{8 \text{ T}}{B} \right), \quad (5)$$

which suggests that the signal in a cavity haloscope is larger. Furthermore, J_{EDM} is more difficult to calculate, as it depends sensitively on nuclear, atomic, and material properties. For these reasons, the polarization haloscope idea was briefly raised and discarded 30 years ago [58]. However, the rapid recent progress in cavity haloscopes motivates a thorough analysis of its potential. In Sec. II we show that $d_A \sim d_n$ can be achieved for certain atoms. We then consider the factors necessary to develop an effective polarization haloscope, such as cavity design (Sec. III), material choice (Sec. IV), and nuclear spin polarization (Sec. V). We estimate experimental sensitivity in Sec. VI

and conclude in Sec. VII, laying out a path towards reaching the QCD axion.

II. AXION-INDUCED EDMs

The dominant nuclear contribution to the EDM of an atom with atomic number Z arises from the \mathcal{P} , \mathcal{T} -violating piece of the effective nuclear electric potential [59–64],

$$\phi_N^{(\text{eff})}(\mathbf{x}) = \left(1 + \frac{1}{Ze} \mathbf{d}_N \cdot \nabla \right) \phi_N(\mathbf{x}), \quad (6)$$

which includes the usual electric potential ϕ_N of the nucleus and the response of the atomic electrons to the nuclear EDM \mathbf{d}_N . The leading \mathcal{P} , \mathcal{T} -violating term in a multipole expansion of $\phi_N^{(\text{eff})}$ is the dipole, but it simply vanishes, in accordance with Schiff's theorem [65] which states that the nuclear EDM is efficiently screened by the atomic electrons. The next \mathcal{P} , \mathcal{T} -violating term is the octupole. Its traceless part corresponds to an electric octupole moment, whose effects are suppressed by the centrifugal barrier near the nucleus [59]. The traceful part yields the dominant contribution to the atomic EDM and is described by the Schiff moment [60],

$$\mathbf{S} = \frac{1}{10} \int d^3\mathbf{x} \rho_N(\mathbf{x}) r^2 \left(\mathbf{x} - \frac{5}{3} \frac{\mathbf{d}_N}{Ze} \right), \quad (7)$$

where ρ_N is the nuclear charge density; \mathbf{S} sources a \mathcal{P} , \mathcal{T} -violating electric field that polarizes the atomic electrons, perturbing the electronic Hamiltonian by

$$V_S = - \sum_{i=1}^Z e \mathbf{S} \cdot \nabla \delta^3(\mathbf{x}_i), \quad (8)$$

where the nucleus is at the origin. The interaction V_S mixes opposite parity states, which to first order in perturbation theory gives rise to a nonvanishing atomic EDM, parallel to the nuclear spin \mathbf{I} , of the form

$$\mathbf{d}_A \simeq \sum_n \frac{\langle n | V_S | 0 \rangle \langle 0 | \mathbf{D} | n \rangle}{E_n - E_0} + \text{H.c.}, \quad (9)$$

where $|n\rangle$ are atomic states of energy E_n and $\mathbf{D} = -\sum_{i=1}^Z e \mathbf{x}_i$ is the atomic EDM operator. The result scales as $d_A \propto Z^2 S$, with a moderate relativistic enhancement for the heaviest nuclei. Scaling numeric results for ^{225}Ra from Refs. [66–69] yields

$$d_A \simeq -(0.27 \times 10^{-3} e \text{ fm}) \langle S_z \rangle / (e \text{ fm}^3) \quad (10)$$

for ^{161}Dy , with values within 20% for the other nuclei we will consider below. Here, $\langle S_z \rangle$ is the lab-frame expectation value of the Schiff moment directed along the nuclear spin for a maximally polarized nucleus, $M = I$ [63].

In perturbation theory, the Schiff moment is

$$\langle S_z \rangle \simeq \sum_n \frac{\langle n | V_{\mathcal{PT}} | 0 \rangle \langle 0 | S_z | n \rangle}{E_n - E_0} + \text{H.c.}, \quad (11)$$

where $|n\rangle$ are nuclear states of energy E_n and $V_{\mathcal{PT}} \propto \theta_a$ is the axion's \mathcal{P} , \mathcal{T} -violating modification to the pion-mediated internucleon interaction. For a typical spherical nucleus with mass number A and radius $R_0 \simeq (1.2 \text{ fm})A^{1/3}$, we expect [59,60]

$$\langle n | V_{\mathcal{PT}} | 0 \rangle \sim (10^{-2} \theta_a / m_n R_0) (A / m_\pi^2 R_0^3), \quad (12)$$

$$\langle 0 | S_z | n \rangle \sim e R_0^3, \quad (13)$$

$$E_n - E_0 \sim A / m_\pi^2 R_0^3, \quad (14)$$

which yields the parametric estimate

$$\langle S_z \rangle \sim 10^{-2} \frac{e R_0^2}{m_n} \theta_a \sim (0.1 \times e \text{ fm}^3) \theta_a \left(\frac{A}{10^2} \right)^{\frac{2}{3}}, \quad (15)$$

in agreement with detailed calculations [26,59,60,70–74].

This yields only a small atomic EDM, $d_A \ll d_n$, but for nonspherical nuclei there can be a large intrinsic Schiff moment S_{int} in the body-fixed frame. Evaluating Eq. (7) gives $S_{\text{int}} \propto \beta_2 \beta_3 Z e R_0^3$, where β_2 and β_3 parametrize the quadrupole and octupole deformation of the nuclear radius. The lab-frame Schiff moment is then determined by averaging over nuclear orientations, $\langle S_z \rangle = S_{\text{int}} \langle \hat{n}_z \rangle$, where $\hat{\mathbf{n}}$ is the nuclear axis. A nonzero $\langle \hat{n}_z \rangle$ requires \mathcal{P} violation and is thus proportional to θ_a . It can be calculated perturbatively with an expression analogous to Eq. (11), the main difference being that octupole deformations imply states with small energy gaps, $E_n - E_0 \sim 50 \text{ keV}$. For significantly octupole-deformed nuclei, $\beta_2 \sim \beta_3 \sim \mathcal{O}(0.1)$, various numeric factors cancel, leaving [70–74]

$$\langle S_z \rangle \sim 10^{-2} \frac{Z e R_0^2}{m_n} \theta_a, \quad (16)$$

which is crucially enhanced by Z relative to Eq. (15). Applying Eq. (10), we find that for these nuclei,

$$|d_A| \sim (\text{few} \times 10^{-3}) e \text{ fm} \times \theta_a \left(\frac{Z}{10^2} \right)^3 \left(\frac{A}{10^2} \right)^{\frac{2}{3}}, \quad (17)$$

which, as anticipated above, is comparable to d_n .

Most octupole-deformed nuclei are short lived and thus infeasible to gather in the macroscopic quantities required. Of the nuclei highlighted in Refs. [69,75,76], we identify ^{161}Dy , ^{153}Eu , and ^{155}Gd as the most promising. They are absolutely stable and, as indicated in Table I, are inexpensive and expected to possess fairly large axion-induced Schiff moments and atomic EDMs. However,

TABLE I. Stable nuclei with large axion-induced Schiff moments $\langle S_z \rangle$ and atomic EDMs d_A , and their natural abundance and price. We use the last row [equal to $|\gamma|(I+1)/3$ where γ is the gyromagnetic ratio [78]] to determine the fractional nuclear spin polarization f_p at a temperature T in a magnetic field B .

	^{161}Dy	^{153}Eu	^{155}Gd
Estimated $\langle S_z \rangle$ ($e \text{ fm}^3 \theta_a$) [75]	4.3	1.0	1.2
Estimated $ d_A $ ($10^{-3} e \text{ fm} \theta_a$)	1.2	0.25	0.3
Natural abundance [79]	19%	52%	15%
Metal price (\$/ton) [80]	300 k	30 k	30 k
$T df_p / dB _{B=0}$ (mK/T) [79]	0.08	0.26	0.05

the existence of octupole deformation in these nuclei is not completely settled [77]. This work motivates further experimental study. Even if none of these nuclei are octupole deformed, it may still be possible to achieve comparable EDMs via magnetic quadrupole moments, which are enhanced by well-established nuclear quadrupole deformations [75].

III. CAVITY EXCITATION

The axion field oscillates with a phase offset and amplitude varying over the coherence time $\tau_a \sim Q_a / m_a$, where $Q_a \sim 10^6$. For all axion masses we consider, spatial gradients of the axion field are negligible. The cavity response is therefore very similar to that of a conventional haloscope, with $\mathbf{J}_{a\gamma\gamma}$ replaced by $\mathbf{J}_{\text{EDM}} \simeq m_a n_A \mathbf{d}_A$. In our case, there is also an associated physical charge density $\rho_{\text{EDM}} = -\nabla \cdot \mathbf{P}_{\text{EDM}}$ in the cavity, which produces small electric fields, but it is not of interest because it cannot excite resonant modes [81–83].

We suppose a portion V_p of the volume V of the cavity is filled with dielectric of fractional nuclear spin polarization f_p along the $\hat{\mathbf{p}}$ direction, so that $n_A = f_p n_0$, where n_0 is the number density of relevant nuclei. Adapting a standard result [84], the power deposited to the i th mode of the cavity on resonance, $m_a \simeq \omega_i$, is

$$P_{\text{sig}} \simeq m_a (f_p n_0 d_A)^2 (V/\bar{\epsilon}) \eta_i^2 \min(Q_a, Q_i), \quad (18)$$

where d_A is now the time-independent amplitude of the atomic EDM, Q_i is the quality factor of the mode, and the last factor accounts for the spectral width of the axion. The typical dielectric permittivity inside the cavity is $\bar{\epsilon}$, and the geometric overlap factor is

$$\eta_i = \frac{|\int_{V_p} d^3 \mathbf{x} \mathbf{E}_i \cdot \hat{\mathbf{p}}|}{\sqrt{V \int_V d^3 \mathbf{x} (\epsilon/\bar{\epsilon}) E_i^2}}. \quad (19)$$

This definition is chosen so that $\eta_i \sim 1$ when the cavity is completely filled with dielectric polarized along $\hat{\mathbf{p}}$ parallel

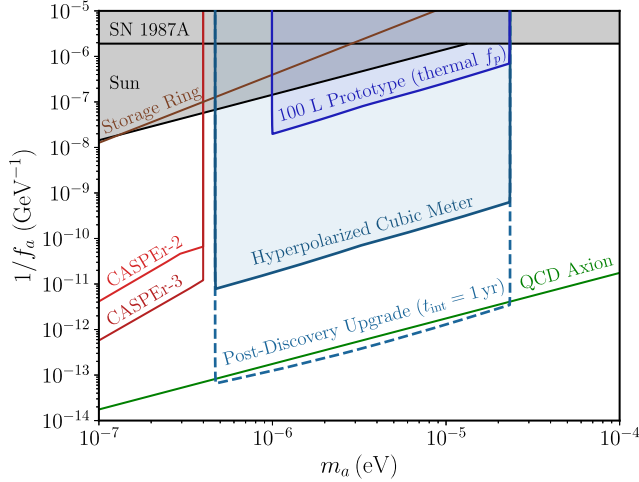


FIG. 2. The projected sensitivity for three benchmark polarization haloscopes (see text for details). The blue shaded regions indicate the reach of scanning setups, while the dashed blue line shows the reach for an experiment which targets a single candidate QCD axion mass. We also show the ultimate projected sensitivity of CASPER-Electric [16] and storage ring [21] experiments, as well as existing constraints from the cooling of Supernova 1987A [114] and Solar fusion processes [115]. Note that these existing constraints are strictly stronger than those derived from Big Bang nucleosynthesis [116] (not shown).

to the electric field \mathbf{E}_i of the cavity mode. Below, we suppress mode subscripts to simplify notation.

To probe the lowest possible axion masses, a cylindrical cavity can be completely filled with a dielectric with $\hat{\mathbf{p}}$ along the cylinder’s axis, which yields $\eta \simeq 0.83$ for the TM_{010} mode. In Fig. 1, we show two concrete ways to guarantee $\mathcal{O}(1)$ geometric overlap for heavier axions coupled to higher resonant modes of the cavity. First, one can insert layers of another dielectric. For example, rutile carries a negligible axion-induced current, and hence does not contribute to V_p . Since it has a very high permittivity at cryogenic temperatures, $\epsilon \gtrsim 10^4$ [85], thin layers would suffice to preserve a large overlap factor. Alternatively, the cavity can be filled with dielectric whose spin polarization alternates in direction. In either case, the mode frequency can be coarsely tuned by changing the number of layers, and finely tuned by introducing gaps and moving the dielectric layers or end caps along the cylinder’s axis.

Such layered structures have been proposed, prototyped, operated, and tuned for haloscopes targeting the axion-photon coupling [86–93]. Axions can also be effectively coupled to higher-order modes by loading cavities with dielectric wedges or cylindrical shells [84,94–98]. At high axion masses, scanning can become impeded by mode crowding. Many innovative approaches have been considered to avoid this issue, such as open resonators [91,92], phase-matched, coupled, or subdivided cavities [39,47,99–108], rod or wire metamaterials [109–111], and

thin-shell geometries [112,113]. Most of these ideas can be adapted to polarization haloscopes, though some tuning mechanisms must be adjusted. For concreteness, we take $\eta = 1$, assume a cylindrical cavity with aspect ratio $L/R = 5$, and require the intermediate layers in Fig. 1 be at least 1 cm thick, so that there is a reasonable number to tune. This determines the mass range probed in Fig. 2.

IV. MATERIAL PROPERTIES

To maximize the signal strength, we consider dielectric materials with a high density of the nuclei in Table I. Unlike other approaches that require the material to be ferroelectric [15] or piezoelectric [26], we only require the material to be insulating at low temperatures.

Some semiconducting or insulating candidate materials are nitrides XN [117], oxides XO , and sesquioxides X_2O_3 for $\text{X} = \text{Dy}, \text{Eu}, \text{Gd}$. Though many alternatives exist, these materials are simple and well studied, and most are commercially available. For a prototype setup, we consider EuN where the abundance of ^{153}Eu is 52% (see Table I). Following other proposals [15,26], we assume complete isotope separation for a full-scale experiment, using DyN where the dysprosium is entirely ^{161}Dy . In both cases, the number density of rare earth atoms is $3 \times 10^{22} \text{ cm}^{-3}$ [118,119].

The structure of the material also directly affects the strength of the signal. The most important effect, displayed in Eq. (18), is that dielectrics shield electric fields, reducing the signal power by a factor of the permittivity $\bar{\epsilon}$. For our projections we take $\bar{\epsilon} \simeq 7$, based on the static permittivity of DyN [120]. This choice is conservative, as permittivity decreases at higher frequencies.

In addition, the effective atomic EDM may be modified within a crystal, where atomic orbitals are deformed. This effect is quantified by the “electroaxionic” tensor defined in Ref. [26], and calculating the tensor components requires a dedicated relativistic many-body calculation for each material. In PbTiO_3 , two groups found suppressions of 25% [121] and 50% [122], but with comparably large uncertainties. Thus, for this initial study we simply take d_A to be the value for an isolated atom.

The other key material property is the dielectric loss tangent $\tan \delta$. For a cavity entirely filled with dielectric, the quality factor Q of a mode obeys $1/Q = 1/Q_c + \tan \delta$, where Q_c is the quality factor due to cavity wall losses. Thus, to realize a desired Q , one must have $\tan \delta \lesssim 1/Q$.

At room temperature, dielectrics display high losses due to thermal phonons. However, these “intrinsic” losses fall steeply with temperature [123], and are negligible at the cryogenic temperatures of polarization haloscopes. Instead, extrinsic losses due to defects and impurities dominate [124,125] and depend on crystal quality. Very low losses have been measured [126–129], at the level of 10^{-9} for sapphire and 10^{-8} for rutile and yttrium aluminum garnet.

These are all centrosymmetric crystals, and thereby avoid additional loss mechanisms that would appear in more complex crystals, e.g., through acoustic phonons in piezoelectrics [123] or domain wall motion in ferroelectrics [130]. The candidate materials we have listed above are also all simple centrosymmetric crystals. However, their dielectric losses are unknown, and dedicated cryogenic measurements in high-quality crystals are needed. These should be carried out at low electric field amplitudes, because high field amplitudes can mask losses due to two-level systems [131–133].

V. NUCLEAR SPIN POLARIZATION

The current in a polarization haloscope is proportional to the fractional nuclear spin polarization f_p , which is $\mathcal{O}(1\%)$ in thermal equilibrium in typical cavity haloscope conditions (see Table I). However, for both polarization haloscopes and other approaches [15,26] an $\mathcal{O}(1)$ polarization is required for optimal sensitivity. Below we describe two potential approaches to realize this.

First, one could simply subject the dielectric to a high magnetic field $B \gtrsim 10$ T and ultralow temperature. At $T = 2$ mK, as achieved by specialized dilution fridges [134,135], ^{153}Eu nuclei possess an $\mathcal{O}(1)$ equilibrium polarization. For this technique, the key unknown is the time needed to thermalize the spins. At such high B/T , theoretical estimates suggest that it is prohibitively long [136,137], but measured spin-lattice relaxation times are much shorter than predicted [138,139], which could be explained by exotic relaxation mechanisms [140–142]. Relaxation times might be further reduced by the electric quadrupole moments of the nuclei we consider, which couple more strongly to the lattice than magnetic dipole moments [143], or by the addition of relaxation agents [144,145].

Another option is frozen spin dynamic nuclear polarization (DNP), in which electrons are polarized in a few-Tesla field at $T \sim 1$ K, and their polarization is transferred to the nuclear spins by applying ~ 1 W/kg of microwave power. This method achieves almost complete proton spin polarization and has been extended to heavier nuclei for nuclear magnetic resonance studies [146–149]. It requires the sample to contain a concentration $\sim 10^{-3}$ of paramagnetic centers, produced by chemical doping or ionizing radiation. To “freeze” the nuclear spins, the microwave field is removed and the sample is further cooled to slow relaxation.

This approach has been used for decades to polarize targets for particle physics experiments [150,151]; notably, the Spin Muon Collaboration at CERN produced frozen spin targets of liter scale [152]. Currently, frozen spin DNP is primarily developed in nuclear physics experiments [153–158]. The resulting spin polarization is robust, with spin-lattice relaxation times of nearly a year observed in practice [159]. For polarization haloscopes, the next step is to see how this approach can be scaled to larger volumes, while maintaining low dielectric losses.

VI. PROJECTED SENSITIVITY

The signal-to-noise ratio (SNR) is given by the Dicke radiometer equation [160],

$$\text{SNR} \simeq \frac{P_{\text{sig}}}{T_n} \sqrt{\frac{t_{\text{int}}}{\Delta\nu_s}}, \quad (20)$$

where t_{int} is the time spent probing each axion mass, and $\Delta\nu_s = m_a / (2\pi \max(Q, Q_a))$ is the signal bandwidth. The noise temperature $T_n = T + T_{\text{amp}}$ receives comparable contributions from thermal noise, determined by the physical temperature T , and amplifier noise. Following Ref. [26], we find that noise due to external vibrations or spin fluctuations is vastly subdominant at the GHz frequencies of interest, even with the inclusion of paramagnetic centers as required for DNP. Note that Q is the quality factor of the cavity mode with dielectric losses included; thus, thermal noise automatically includes both the noise from electrons in the cavity walls and dielectric noise, by the fluctuation-dissipation theorem.

In Fig. 2, we show the projected sensitivity (corresponding to $\text{SNR} \geq 2$) for three experimental setups. The two blue shaded regions indicate scanning setups which take frequency steps of size $m_a / \min(Q, Q_a)$ with a uniform t_{int} , so that one e -fold in axion mass is scanned in one year. Following existing haloscope experiments, we assume an operating temperature of $T = 40$ mK [40] and an amplifier operating at the quantum limit, $T_{\text{amp}} \simeq m_a$. When thermal noise dominates, we assume the cavity is optimally over-coupled to the readout, which modestly improves the SNR by a factor of $\sqrt{T/T_{\text{amp}}}$ [161].

The “prototype” projection, shown in dark blue, is modeled on the ADMX haloscope [34] and assumes a volume $V = 100\text{L}$, quality factor $Q = 10^5$, and magnetic field $B = 8$ T, which produces a thermal spin polarization $f_p \simeq 5\%$ for ^{153}Eu . This benchmark shows that new parameter space can be explored with minimal investment. (However, this parameter space may be in tension with the stability of white dwarfs [162].)

The light blue projection considers a cubic meter cavity with $Q = 10^6$ and complete spin polarization, $f_p = 1$. Such an experiment would require a large dilution fridge, like those developed for other precision experiments [163–167], and several tons of dielectric material. In other words, it would require investment comparable to ongoing weakly interacting massive particle (WIMP) dark matter searches [168,169]. Though it does not reach the canonical QCD axion line defined by Eq. (2), it could probe orders of magnitude of unexplored parameter space, including nonminimal, mildly tuned QCD axion models which solve the strong CP problem with exponentially smaller $m_a f_a$ [170,171].

If ADMX, CAPP, or any other GHz-frequency haloscope [172–176] detects a signal consistent with axion dark matter, a “post-discovery” setup, shown in dashed blue,

can probe the same mass. Since it sits at a single frequency, the SNR is enhanced by $Q_a^{1/2} \sim 10^3$ for $t_{\text{int}} = 1$ yr, as compared to a scanning experiment. We assume noise is reduced, relative to the cuber meter setup, by cooling to 10 mK and reducing amplifier noise by 3 dB using demonstrated vacuum squeezing techniques [37]. We also assume a quality factor of $Q = 10^8$. To achieve this quality factor, one needs a material with $\tan \delta \lesssim 10^{-8}$, which has been measured for a number of compounds. As for wall losses, one can achieve $Q_c \gg 10^8$ with a superconducting cavity, since polarization haloscopes do not require large static magnetic fields. Alternatively, the mode profile can be shaped with dielectrics, a technique which has achieved $Q \sim 10^7$ in a liter-scale copper cavity [97]. With these enhancements, a polarization haloscope has the unique ability to probe the minimal QCD axion.

VII. DISCUSSION

The QCD axion is an exceptional dark matter candidate, which arises automatically in theories which solve other problems of the Standard Model, with a simple and predictive production mechanism. The minimal QCD axion also has the unique advantage of possessing a defining coupling to the Standard Model, which provides a sharp target for laboratory searches.

A polarization haloscope naturally targets higher frequencies than nuclear magnetic resonance experiments [15]. Both approaches detect the electromagnetic fields generated by spin polarized nuclei, but polarization

haloscopes do not involve changes in the spin direction and hence do not require long spin coherence times. One could also target kHz to MHz frequencies with our approach by replacing the magnetic field in an LC circuit haloscope [177–179] with a polarized dielectric.

We have laid out a path towards definitively probing the QCD axion with polarization haloscopes. No fundamentally new technologies are required, but many uncertainties remain. Precisely computing the signal requires expertise in theoretical nuclear, atomic, and solid state physics, while the cavity design and the selection and polarization of the material require experimental investigation. Together, such efforts may enable the next definitive search for dark matter.

ACKNOWLEDGMENTS

We thank John Behr, Raphael Cervantes, Andrei Derevianko, Victor Flambaum, Roni Harnik, Anson Hook, Yoni Kahn, Amalia Madden, Surjeet Rajendran, Gray Rybka, Alex Sushkov, and Natalia Toro for helpful discussions. This material is based upon work supported by the U.S. Department of Energy, Office of Science, National Quantum Information Science Research Centers, Superconducting Quantum Materials and Systems Center (SQMS) under Contract No. DE-AC02-07CH11359. Fermilab is operated by the Fermi Research Alliance, LLC under Contract No. DEAC02-07CH11359 with the U. S. Department of Energy. K.Z. is supported by the National Science Foundation's Graduate Research Fellowship Program under Grant No. DGE-1656518.

-
- [1] R. D. Peccei and H. R. Quinn, *CP Conservation in the Presence of Instantons*, *Phys. Rev. Lett.* **38**, 1440 (1977).
 - [2] R. D. Peccei and H. R. Quinn, *Constraints imposed by CP conservation in the presence of instantons*, *Phys. Rev. D* **16**, 1791 (1977).
 - [3] S. Weinberg, *A New Light Boson?*, *Phys. Rev. Lett.* **40**, 223 (1978).
 - [4] F. Wilczek, *Problem of Strong P and T Invariance in the Presence of Instantons*, *Phys. Rev. Lett.* **40**, 279 (1978).
 - [5] J. Preskill, M. B. Wise, and F. Wilczek, *Cosmology of the invisible axion*, *Phys. Lett.* **120B**, 127 (1983).
 - [6] L. F. Abbott and P. Sikivie, *A cosmological bound on the invisible axion*, *Phys. Lett.* **120B**, 133 (1983).
 - [7] M. Dine and W. Fischler, *The not so harmless axion*, *Phys. Lett.* **120B**, 137 (1983).
 - [8] C. Abel *et al.*, *Measurement of the Permanent Electric Dipole Moment of the Neutron*, *Phys. Rev. Lett.* **124**, 081803 (2020).
 - [9] G. Grilli di Cortona, E. Hardy, J. Pardo Vega, and G. Villadoro, *The QCD axion, precisely*, *J. High Energy Phys.* **01** (2016) 034.
 - [10] S. Borsanyi *et al.*, *Calculation of the axion mass based on high-temperature lattice quantum chromodynamics*, *Nature (London)* **539**, 69 (2016).
 - [11] M. Pospelov and A. Ritz, *Theta Induced Electric Dipole Moment of the Neutron via QCD Sum Rules*, *Phys. Rev. Lett.* **83**, 2526 (1999).
 - [12] C. Abel *et al.*, *Search for Axionlike Dark Matter through Nuclear Spin Precession in Electric and Magnetic Fields*, *Phys. Rev. X* **7**, 041034 (2017).
 - [13] T. S. Roussy *et al.*, *Experimental Constraint on Axionlike Particles over Seven Orders of Magnitude in Mass*, *Phys. Rev. Lett.* **126**, 171301 (2021).
 - [14] I. Schulthess *et al.*, *New Limit on Axion-Dark-Matter using Cold Neutrons*, *Phys. Rev. Lett.* **129**, 191801 (2022).
 - [15] D. Budker, P. W. Graham, M. Ledbetter, S. Rajendran, and A. Sushkov, *Proposal for a Cosmic Axion Spin Precession Experiment (CASPER)*, *Phys. Rev. X* **4**, 021030 (2014).
 - [16] D. F. Jackson Kimball *et al.*, *Overview of the cosmic axion spin precession experiment (CASPER)*, *Springer Proc. Phys.* **245**, 105 (2020).

- [17] D. Aybas *et al.*, Search for Axionlike Dark Matter Using Solid-State Nuclear Magnetic Resonance, *Phys. Rev. Lett.* **126**, 141802 (2021).
- [18] S. P. Chang, S. Haciomeroglu, O. Kim, S. Lee, S. Park, and Y. K. Semertzidis, Axionlike dark matter search using the storage ring EDM method, *Phys. Rev. D* **99**, 083002 (2019).
- [19] J. Pretz, S. Karanth, E. Stephenson, S. P. Chang, V. Hejny, S. Park, Y. Semertzidis, and H. Ströher, Statistical sensitivity estimates for oscillating electric dipole moment measurements in storage rings, *Eur. Phys. J. C* **80**, 107 (2020).
- [20] E. Stephenson (JEDI Collaboration), A search for axionlike particles with a horizontally polarized beam in a storage ring, *Proc. Sci. PSTP2019* (2020) 018.
- [21] O. Kim and Y. K. Semertzidis, New method of probing an oscillating EDM induced by axionlike dark matter using an rf Wien filter in storage rings, *Phys. Rev. D* **104**, 096006 (2021).
- [22] J. Alexander *et al.*, The storage ring proton EDM experiment, [arXiv:2205.00830](https://arxiv.org/abs/2205.00830).
- [23] S. Karanth *et al.*, First Search for Axion-Like Particles in a Storage Ring Using a Polarized Deuteron Beam, *Phys. Rev. X* **13**, 031004 (2023).
- [24] P. W. Graham and S. Rajendran, Axion dark matter detection with cold molecules, *Phys. Rev. D* **84**, 055013 (2011).
- [25] H. Kim and G. Perez, Oscillations of atomic energy levels induced by QCD axion dark matter, [arXiv:2205.12988](https://arxiv.org/abs/2205.12988).
- [26] A. Arvanitaki, A. Madden, and K. Van Tilburg, The piezoaxionic effect, [arXiv:2112.11466](https://arxiv.org/abs/2112.11466).
- [27] P. Sikivie, Experimental Tests of the Invisible Axion, *Phys. Rev. Lett.* **51**, 1415 (1983); *Phys. Rev. Lett.* **52**, 695(E) (1984).
- [28] F. Wilczek, Two Applications of Axion Electrodynamics, *Phys. Rev. Lett.* **58**, 1799 (1987).
- [29] I. G. Irastorza and J. Redondo, New experimental approaches in the search for axion-like particles, *Prog. Part. Nucl. Phys.* **102**, 89 (2018).
- [30] P. Sikivie, Invisible axion search methods, *Rev. Mod. Phys.* **93**, 015004 (2021).
- [31] Y. K. Semertzidis and S. Youn, Axion dark matter: How to see it?, *Sci. Adv.* **8**, abm9928 (2022).
- [32] N. Du *et al.* (ADMX Collaboration), Search for Invisible Axion Dark Matter with the Axion Dark Matter Experiment, *Phys. Rev. Lett.* **120**, 151301 (2018).
- [33] T. Braine *et al.* (ADMX Collaboration), Extended Search for the Invisible Axion with the Axion Dark Matter Experiment, *Phys. Rev. Lett.* **124**, 101303 (2020).
- [34] C. Bartram *et al.* (ADMX Collaboration), Search for Invisible Axion Dark Matter in the 3.3–4.2 μeV Mass Range, *Phys. Rev. Lett.* **127**, 261803 (2021).
- [35] B. M. Brubaker *et al.*, First Results from a Microwave Cavity Axion Search at 24 μeV , *Phys. Rev. Lett.* **118**, 061302 (2017).
- [36] L. Zhong *et al.* (HAYSTAC Collaboration), Results from phase 1 of the HAYSTAC microwave cavity axion experiment, *Phys. Rev. D* **97**, 092001 (2018).
- [37] K. M. Backes *et al.* (HAYSTAC Collaboration), A quantum-enhanced search for dark matter axions, *Nature (London)* **590**, 238 (2021).
- [38] S. Lee, S. Ahn, J. Choi, B. R. Ko, and Y. K. Semertzidis, Axion Dark Matter Search Around 6.7 μeV , *Phys. Rev. Lett.* **124**, 101802 (2020).
- [39] J. Jeong, S. Youn, S. Bae, J. Kim, T. Seong, J. E. Kim, and Y. K. Semertzidis, Search for Invisible Axion Dark Matter with a Multiple-Cell Haloscope, *Phys. Rev. Lett.* **125**, 221302 (2020).
- [40] O. Kwon *et al.* (CAPP Collaboration), First Results from an Axion Haloscope at CAPP around 10.7 μeV , *Phys. Rev. Lett.* **126**, 191802 (2021).
- [41] Y. Lee, B. Yang, H. Yoon, M. Ahn, H. Park, B. Min, D. Kim, and J. Yoo, Searching for Invisible Axion Dark Matter with an 18 T Magnet Haloscope, *Phys. Rev. Lett.* **128**, 241805 (2022).
- [42] J. Kim *et al.*, Near-Quantum-Noise Axion Dark Matter Search at CAPP Around 9.5 μeV , *Phys. Rev. Lett.* **130**, 091602 (2023).
- [43] C. Boutan *et al.* (ADMX Collaboration), Piezoelectrically Tuned Multimode Cavity Search for Axion Dark Matter, *Phys. Rev. Lett.* **121**, 261302 (2018).
- [44] T. Grenet, R. Ballou, Q. Basto, K. Martineau, P. Perrier, P. Pagnat, J. Quevillon, N. Roch, and C. Smith, The Grenoble axion haloscope platform (GrAHal): Development plan and first results, [arXiv:2110.14406](https://arxiv.org/abs/2110.14406).
- [45] H. Chang *et al.* (TASEH Collaboration), Taiwan axion search experiment with haloscope: Designs and operations, *Rev. Sci. Instrum.* **93**, 084501 (2022).
- [46] H. Chang *et al.* (TASEH Collaboration), First Results from the Taiwan Axion Search Experiment with a Haloscope at 19.6 μeV , *Phys. Rev. Lett.* **129**, 111802 (2022).
- [47] A. A. Melcón *et al.* (CAST Collaboration), First results of the CAST-RADES haloscope search for axions at 34.67 μeV , *J. High Energy Phys.* **10** (2021) 75.
- [48] D. Alesini *et al.*, Search for invisible axion dark matter of mass $m_a = 43 \mu\text{eV}$ with the QUAX- γ experiment, *Phys. Rev. D* **103**, 102004 (2021).
- [49] B. T. McAllister, G. Flower, J. Kruger, E. N. Ivanov, M. Goryachev, J. Bourhill, and M. E. Tobar, The ORGAN experiment: An axion haloscope above 15 GHz, *Phys. Dark Universe* **18**, 67 (2017).
- [50] A. P. Quiskamp, B. T. McAllister, P. Altin, E. N. Ivanov, M. Goryachev, and M. E. Tobar, Direct search for dark matter axions excluding ALP cogenesis in the 63- to 67- μeV range with the ORGAN experiment, *Sci. Adv.* **8**, abq3765 (2022).
- [51] D. B. Kaplan, Opening the axion window, *Nucl. Phys.* **260**, B215 (1985).
- [52] S. L. Cheng, C. Q. Geng, and W. T. Ni, Axion-photon couplings in invisible axion models, *Phys. Rev. D* **52**, 3132 (1995).
- [53] L. Di Luzio, F. Mescia, and E. Nardi, Redefining the Axion Window, *Phys. Rev. Lett.* **118**, 031801 (2017).
- [54] L. Di Luzio, F. Mescia, and E. Nardi, Window for preferred axion models, *Phys. Rev. D* **96**, 075003 (2017).
- [55] V. V. Flambaum and H. B. Tran Tan, Oscillating nuclear electric dipole moment induced by axion dark matter produces atomic and molecular electric dipole moments and nuclear spin rotation, *Phys. Rev. D* **100**, 111301 (2019).

- [56] A. R. Zhitnitsky, On possible suppression of the axion hadron interactions (in Russian), *Sov. J. Nucl. Phys.* **31**, 260 (1980), <https://www.osti.gov/biblio/7063072>.
- [57] M. Dine, W. Fischler, and M. Srednicki, A simple solution to the strong CP Problem with a harmless axion, *Phys. Lett. B* **104**, 199 (1981).
- [58] J. Hong, J. E. Kim, and P. Sikivie, Nuclear dipole radiation from $\bar{\theta}$ oscillations, *Phys. Rev. D* **42**, 1847 (1990).
- [59] I. B. Khriplovich and S. K. Lamoreaux, *CP Violation Without Strangeness: Electric Dipole Moments of Particles, Atoms, and Molecules* (Springer, Berlin, 1997).
- [60] V. V. Flambaum, I. B. Khriplovich, and O. P. Sushkov, On the possibility to study P odd and T odd nuclear forces in atomic and molecular experiments, *Sov. Phys. JETP* **60**, 873 (1984), <https://www.osti.gov/biblio/5511886>.
- [61] J. Engel, J. L. Friar, and A. C. Hayes, Nuclear octupole correlations and the enhancement of atomic time reversal violation, *Phys. Rev. C* **61**, 035502 (2000).
- [62] N. Auerbach, V. V. Flambaum, and V. Spevak, Collective T - and P -Odd Electromagnetic Moments in Nuclei with Octupole Deformations, *Phys. Rev. Lett.* **76**, 4316 (1996).
- [63] V. Spevak, N. Auerbach, and V. V. Flambaum, Enhanced T -odd, P -odd electromagnetic moments in reflection asymmetric nuclei, *Phys. Rev. C* **56**, 1357 (1997).
- [64] J. S. M. Ginges and V. V. Flambaum, Violations of fundamental symmetries in atoms and tests of unification theories of elementary particles, *Phys. Rep.* **397**, 63 (2004).
- [65] L. I. Schiff, Measurability of nuclear electric dipole moments, *Phys. Rev.* **132**, 2194 (1963).
- [66] V. A. Dzuba, V. V. Flambaum, J. S. M. Ginges, and M. G. Kozlov, Electric dipole moments of Hg, Xe, Rn, Ra, Pu, and Tl induced by the nuclear Schiff moment and limits on time reversal violating interactions, *Phys. Rev. A* **66**, 012111 (2002).
- [67] V. A. Dzuba, V. V. Flambaum, and S. G. Porsev, Calculation of (P, T) -odd electric dipole moments for the diamagnetic atoms ^{129}Xe , ^{171}Yb , ^{199}Hg , ^{211}Rn , and ^{225}Ra , *Phys. Rev. A* **80**, 032120 (2009).
- [68] V. A. Dzuba, V. V. Flambaum, and J. S. M. Ginges, Atomic electric dipole moments of He and Yb induced by nuclear Schiff moments, *Phys. Rev. A* **76**, 034501 (2007).
- [69] V. V. Flambaum and H. Feldmeier, Enhanced nuclear Schiff moment in stable and metastable nuclei, *Phys. Rev. C* **101**, 015502 (2020).
- [70] V. F. Dmitriev, I. B. Khriplovich, and V. B. Telitsin, Nuclear magnetic quadrupole moments in the single-particle approximation, *Phys. Rev. C* **50**, 2358 (1994).
- [71] J. de Vries, E. Epelbaum, L. Girlanda, A. Gnech, E. Mereghetti, and M. Viviani, Parity- and time-reversal-violating nuclear forces, *Front. Phys.* **8**, 218 (2020).
- [72] V. V. Flambaum, D. DeMille, and M. G. Kozlov, Time-Reversal Symmetry Violation in Molecules Induced by Nuclear Magnetic Quadrupole Moments, *Phys. Rev. Lett.* **113**, 103003 (2014).
- [73] W. C. Haxton and E. M. Henley, Enhanced T -Nonconserving Nuclear Moments, *Phys. Rev. Lett.* **51**, 1937 (1983).
- [74] A. Griffiths and P. Vogel, One-body parity and time reversal violating potentials, *Phys. Rev. C* **43**, 2844 (1991).
- [75] F. Dalton, V. V. Flambaum, and A. J. Mansour, Enhanced Schiff and magnetic quadrupole moments in deformed nuclei and their connection to the search for axion dark matter, *Phys. Rev. C* **107**, 035502 (2023).
- [76] V. V. Flambaum and V. A. Dzuba, Electric dipole moments of atoms and molecules produced by enhanced nuclear Schiff moments, *Phys. Rev. A* **101**, 042504 (2020).
- [77] J. A. Behr, Nuclei with enhanced Schiff moments in practical elements for atomic and molecular EDM measurements, [arXiv:2203.06758](https://arxiv.org/abs/2203.06758).
- [78] K. F. Stupic, Z. I. Cleveland, G. E. Pavlovskaya, and T. Meersmann, Hyperpolarized ^{131}Xe NMR spectroscopy, *J. Magn. Reson.* **208**, 58 (2011).
- [79] R. K. Harris, E. D. Becker, S. M. C. De Menezes, R. Goodfellow, and P. Granger, NMR nomenclature. Nuclear spin properties and conventions for chemical shifts (IUPAC recommendations 2001), *Pure Appl. Chem.* **73**, 1795 (2001).
- [80] Institute for Rare Earths and Metals, Rare earth prices in February 2020, <https://en.institut-seltene-erden.de/rare-earth-prices-in-february-2020/> (accessed: 2022-08-10).
- [81] E. U. Condon, Forced oscillations in cavity resonators, *J. Appl. Phys.* **12**, 129 (1941).
- [82] W. B. Smythe, *Static and Dynamic Electricity* (Hemisphere Publishing, New York, 1988).
- [83] R. E. Collin, *Field Theory of Guided Waves* (John Wiley & Sons, New York, 1990), Vol. 5.
- [84] J. Kim, S. Youn, J. Jeong, W. Chung, O. Kwon, and Y. K. Semertzidis, Exploiting higher-order resonant modes for axion haloscopes, *J. Phys. G* **47**, 035203 (2020).
- [85] R. A. Parker, Static dielectric constant of rutile (TiO_2), 1.6–1060 °K, *Phys. Rev.* **124**, 1719 (1961).
- [86] D. E. Morris, An electromagnetic detector for relic axions, Lawrence Berkeley National Lab. Report No. LBL-17915, 1984, <https://www.osti.gov/biblio/6446664>.
- [87] P. Sikivie, D. B. Tanner, and Y. Wang, Axion detection in the 10^{-4} eV mass range, *Phys. Rev. D* **50**, 4744 (1994).
- [88] G. Rybka, A. Wagner, A. Brill, K. Ramos, R. Percival, and K. Patel, Search for dark matter axions with the Orpheus experiment, *Phys. Rev. D* **91**, 011701 (2015).
- [89] B. Phillips, The electric tiger experiment: A proof-of-concept for the periodic dielectric loaded resonator, in *Talk given at the 2nd Workshop on Microwave Cavities and Detectors for Axion Research* (2017), https://indico.fnal.gov/event/13068/contributions/17077/attachments/11455/14632/etig_llnl_presentation.pdf.
- [90] J. Egge, S. Knirck, B. Majorovits, C. Moore, and O. Reimann, A first proof of principle booster setup for the MADMAX dielectric haloscope, *Eur. Phys. J. C* **80**, 392 (2020).
- [91] R. Cervantes *et al.*, Search for 70 μeV Dark Photon Dark Matter with a Dielectrically-Loaded Multi-Wavelength Microwave Cavity, *Phys. Rev. Lett.* **129**, 201301 (2022).
- [92] R. Cervantes *et al.*, ADMX-Orpheus first search for 70 μeV dark photon dark matter: Detailed design, operations, and analysis, *Phys. Rev. D* **106**, 102002 (2022).
- [93] C. Lee and O. Reimann, T-RAX: Transversely resonant axion experiment, *J. Cosmol. Astropart. Phys.* **09** (2022) 007.

- [94] A. P. Quiskamp, B. T. McAllister, G. Rybka, and M. E. Tobar, Dielectric-Boosted Sensitivity to Cylindrical Azimuthally Varying Transverse-Magnetic Resonant Modes in an Axion Haloscope, *Phys. Rev. Appl.* **14**, 044051 (2020).
- [95] B. T. McAllister, G. Flower, L. E. Tobar, and M. E. Tobar, Tunable Supermode Dielectric Resonators for Axion Dark-Matter Haloscopes, *Phys. Rev. Appl.* **9**, 014028 (2018).
- [96] D. Alesini *et al.* (QUAX Collaboration), Realization of a high quality factor resonator with hollow dielectric cylinders for axion searches, *Nucl. Instrum. Methods Phys. Res., Sect. A* **985**, 164641 (2021).
- [97] R. Di Vora *et al.*, High- Q Microwave Dielectric Resonator for Axion Dark-Matter Haloscopes, *Phys. Rev. Appl.* **17**, 054013 (2022).
- [98] D. Alesini *et al.*, Search for Galactic axions with a high- Q dielectric cavity, *Phys. Rev. D* **106**, 052007 (2022).
- [99] J. Jeong, S. Youn, S. Ahn, C. Kang, and Y. K. Semertzidis, Phase-matching of multiple-cavity detectors for dark matter axion search, *Astropart. Phys.* **97**, 33 (2018).
- [100] J. Yang, J. R. Gleason, S. Jois, I. Stern, P. Sikivie, N. S. Sullivan, and D. B. Tanner, Search for 5–9 μeV axions with ADMX four-cavity array, *Springer Proc. Phys.* **245**, 53 (2020).
- [101] M. Maroudas, Search for dark matter axions with CAST-CAPP, in *Talk given at the 16th Patras Workshop on Axions, WIMPs and WISPs* (2021), https://agenda.infn.it/event/20431/contributions/137685/attachments/82563/108509/2021_06_14%20-%20Patras%20Workshop%20Presentation.pdf.
- [102] M. Goryachev, B. T. McAllister, and M. E. Tobar, Axion detection with negatively coupled cavity arrays, *Phys. Lett. A* **382**, 2199 (2018).
- [103] A. A. Melcón *et al.*, Axion searches with microwave filters: The RADES project, *J. Cosmol. Astropart. Phys.* **05** (2018) 040.
- [104] S. Arguedas Cuendis *et al.*, The 3 cavity prototypes of RADES: An axion detector using microwave filters at CAST, *Springer Proc. Phys.* **245**, 45 (2020).
- [105] A. Álvarez Melcón *et al.*, Scalable haloscopes for axion dark matter detection in the 30 μeV range with RADES, *J. High Energy Phys.* **07** (2020) 084.
- [106] A. Díaz-Morcillo *et al.*, Design of new resonant haloscopes in the search for the dark matter axion: A review of the first steps in the RADES Collaboration, *Universe* **8**, 5 (2021).
- [107] J. Jeong, S. Youn, S. Ahn, J. E. Kim, and Y. K. Semertzidis, Concept of multiple-cell cavity for axion dark matter search, *Phys. Lett. B* **777**, 412 (2018).
- [108] J. Jeong, S. Youn, and J. E. Kim, Multiple-cell cavity design for high mass axion searches: An extended study, *Nucl. Instrum. Methods Phys. Res., Sect. A* **1053**, 168327 (2023).
- [109] M. Lawson, A. J. Millar, M. Pancaldi, E. Vitagliano, and F. Wilczek, Tunable Axion Plasma Haloscopes, *Phys. Rev. Lett.* **123**, 141802 (2019).
- [110] M. Wooten, A. Droster, A. Kenany, D. Sun, S. M. Lewis, and K. van Bibber, Exploration of wire array metamaterials for the plasma axion haloscope, [arXiv:2203.13945](https://arxiv.org/abs/2203.13945).
- [111] S. Bae, S. Youn, and J. Jeong, Tunable photonic crystal haloscope for high-mass axion searches, *Phys. Rev. D* **107**, 015012 (2023).
- [112] C.-L. Kuo, Large-volume centimeter-wave cavities for axion searches, *J. Cosmol. Astropart. Phys.* **06** (2020) 010.
- [113] C.-L. Kuo, Symmetrically tuned large-volume conic shell-cavities for axion searches, *J. Cosmol. Astropart. Phys.* **02** (2021) 018.
- [114] G. Lucente, L. Mastrototaro, P. Carezza, L. Di Luzio, M. Giannotti, and A. Mirizzi, Axion signatures from supernova explosions through the nucleon electric-dipole portal, *Phys. Rev. D* **105**, 123020 (2022).
- [115] A. Hook and J. Huang, Probing axions with neutron star inspirals and other stellar processes, *J. High Energy Phys.* **06** (2018) 036.
- [116] K. Blum, R. T. D’Agnolo, M. Lisanti, and B. R. Safdi, Constraining axion dark matter with big bang nucleosynthesis, *Phys. Lett. B* **737**, 30 (2014).
- [117] F. Natali, B. J. Ruck, N. O. Plank, H. J. Trodahl, S. Granville, C. Meyer, and W. R. Lambrecht, Rare-earth mononitrides, *Prog. Mater. Sci.* **58**, 1316 (2013).
- [118] A. Jain, S. P. Ong, G. Hautier, W. Chen, W. D. Richards, S. Dacek, S. Cholia, D. Gunter, D. Skinner, G. Ceder, and K. A. Persson, Commentary: The Materials Project: A materials genome approach to accelerating materials innovation, *APL Mater.* **1**, 011002 (2013).
- [119] I. Petousis, D. Mrdjenovich, E. Ballouz, M. Liu, D. Winston, W. Chen, T. Graf, T. D. Schladt, K. A. Persson, and F. B. Prinz, High-throughput screening of inorganic compounds for the discovery of novel dielectric and optical materials, *Sci. Data* **4**, 1 (2017).
- [120] D. Xue, K. Betzler, and H. Hesse, Dielectric constants of binary rare-earth compounds, *J. Phys. Condens. Matter* **12**, 3113 (2000).
- [121] L. V. Skripnikov and A. V. Titov, LCAO-based theoretical study of PbTiO_3 crystal to search for parity and time reversal violating interaction in solids, *J. Chem. Phys.* **145**, 054115 (2016).
- [122] J. A. Ludlow and O. P. Sushkov, Investigating the nuclear Schiff moment of ^{207}Pb in ferroelectric PbTiO_3 , *J. Phys. B* **46**, 085001 (2013).
- [123] V. Gurevich and A. Tagantsev, Intrinsic dielectric loss in crystals, *Adv. Phys.* **40**, 719 (1991).
- [124] N. M. Alford, J. Breeze, X. Wang, S. Penn, S. Dalla, S. Webb, N. Ljepojevic, and X. Aupi, Dielectric loss of oxide single crystals and polycrystalline analogues from 10 to 320 K, *J. Eur. Ceram. Soc.* **21**, 2605 (2001).
- [125] X. Aupi, J. Breeze, N. Ljepojevic, L. J. Dunne, N. Malde, A.-K. Axelsson, and N. M. Alford, Microwave dielectric loss in oxides: Theory and experiment, *J. Appl. Phys.* **95**, 2639 (2004).
- [126] V. Braginsky, V. Ilchenko, and K. S. Bagdassarov, Experimental observation of fundamental microwave absorption in high-quality dielectric crystals, *Phys. Lett.* **120A**, 300 (1987).
- [127] M. E. Tobar, J. Krupka, E. N. Ivanov, and R. A. Woode, Anisotropic complex permittivity measurements

- of mono-crystalline rutile between 10 and 300 K, *J. Appl. Phys.* **83**, 1604 (1998).
- [128] J. Krupka, K. Derzakowski, A. Abramowicz, M. E. Tobar, and R. G. Geyer, Use of whispering-gallery modes for complex permittivity determinations of ultra-low-loss dielectric materials, *IEEE Trans. Microwave Theory Tech.* **47**, 752 (1999).
- [129] J. Krupka, K. Derzakowski, M. Tobar, J. Hartnett, and R. G. Geyer, Complex permittivity of some ultralow loss dielectric crystals at cryogenic temperatures, *Meas. Sci. Technol.* **10**, 387 (1999).
- [130] G. Liu, S. Zhang, W. Jiang, and W. Cao, Losses in ferroelectric materials, *Mater. Sci. Eng.* **89**, 1 (2015).
- [131] J. M. Martinis, K. B. Cooper, R. McDermott, M. Steffen, M. Ansmann, K. D. Osborn, K. Cicak, S. Oh, D. P. Pappas, R. W. Simmonds, and C. C. Yu, Decoherence in Josephson Qubits from Dielectric Loss, *Phys. Rev. Lett.* **95**, 210503 (2005).
- [132] A. D. O'Connell, M. Ansmann, R. C. Bialczak, M. Hofheinz, N. Katz, E. Lucero, C. McKenney, M. Neeley, H. Wang, E. M. Weig *et al.*, Microwave dielectric loss at single photon energies and millikelvin temperatures, *Appl. Phys. Lett.* **92**, 112903 (2008).
- [133] N. Kostylev, M. Goryachev, A. D. Bulanov, V. A. Gavva, and M. E. Tobar, Determination of low loss in isotopically pure single crystal ^{28}Si at low temperatures and single microwave photon energy, *Sci. Rep.* **7**, 44813 (2017).
- [134] D. S. Betts, *An Introduction to Millikelvin Technology*, Cambridge Studies in Low Temperature Physics (Cambridge University Press, Cambridge, England, 1989).
- [135] H. Zu, W. Dai, and A. de Waele, Development of dilution refrigerators—a review, *Cryogenics* **121**, 103390 (2022).
- [136] A. Abragam and M. Goldman, *Nuclear Magnetism: Order and Disorder* (Clarendon Press, Oxford, 1982).
- [137] O. Gonen and J. Waugh, NMR relaxation mechanisms and line widths in insulators below 1 K, *Physica (Amsterdam)* **156A**, 219 (1989).
- [138] W. de Boer and T. Niinikoski, Dynamic proton polarization in propanediol below 0.5 K, *Nucl. Instrum. Methods* **114**, 495 (1974).
- [139] P. Kuhns, P. Hammel, O. Gonen, and J. Waugh, Unexpectedly rapid ^{19}F spin-lattice relaxation in CaF_2 below 1 K, *Phys. Rev. B* **35**, 4591 (1987).
- [140] J. Waugh and C. P. Slichter, Mechanism of nuclear spin-lattice relaxation in insulators at very low temperatures, *Phys. Rev. B* **37**, 4337 (1988).
- [141] P. Phillips, D. Izzo, and K. Kundu, Spin-lattice relaxation below 1 K: A new mechanism for unexpected nuclear spin relaxation, *Phys. Rev. B* **37**, 10876 (1988).
- [142] A. J. Vega, P. A. Beckmann, S. Bai, and C. Dybowski, Spin-lattice relaxation of heavy spin-1/2 nuclei in diamagnetic solids: A Raman process mediated by spin-rotation interaction, *Phys. Rev. B* **74**, 214420 (2006).
- [143] A. Abragam, *The Principles of Nuclear Magnetism*, No. 32 in International Series of Monographs on Physics (Clarendon Press, Oxford, 1961).
- [144] E. Krjukov, J. O'Neill, and J. Owers-Bradley, Brute force polarization of ^{129}Xe , *J. Low Temp. Phys.* **140**, 397 (2005).
- [145] J. R. Owers-Bradley, A. J. Horsewill, D. T. Peat, K. S. Goh, and D. G. Gadian, High polarization of nuclear spins mediated by nanoparticles at millikelvin temperatures, *Phys. Chem. Chem. Phys.* **15**, 10413 (2013).
- [146] J. H. Ardenkjær-Larsen, B. Fridlund, A. Gram, G. Hansson, L. Hansson, M. H. Lerche, R. Servin, M. Thaning, and K. Golman, Increase in signal-to-noise ratio of >10,000 times in liquid-state NMR, *Proc. Natl. Acad. Sci. U.S.A.* **100**, 10158 (2003).
- [147] D. Lee, S. Hediger, and G. De Paëpe, Is solid-state NMR enhanced by dynamic nuclear polarization?, *Solid State Nucl. Magn. Reson.* **66**, 6 (2015).
- [148] J. H. Ardenkjær-Larsen, On the present and future of dissolution-DNP, *J. Magn. Reson.* **264**, 3 (2016).
- [149] J. Eills *et al.*, Spin hyperpolarization in modern magnetic resonance, *Chem. Rev.* **123**, 1417 (2023).
- [150] D. G. Crabb and W. Meyer, Solid polarized targets for nuclear and particle physics experiments, *Annu. Rev. Nucl. Part. Sci.* **47**, 67 (1997).
- [151] S. Goertz, W. Meyer, and G. Reicherz, Polarized H, D and He-3 targets for particle physics experiments, *Prog. Part. Nucl. Phys.* **49**, 403 (2002); *Prog. Part. Nucl. Phys.* **51**, 309 (E) (2003).
- [152] D. Adams *et al.* (Spin Muon Collaboration), The polarized double cell target of the SMC, *Nucl. Instrum. Methods Phys. Res., Sect. A* **437**, 23 (1999).
- [153] C. Keith, Polarized solid targets: Recent progress and future prospects, *Polarized Sources, Targets And Polarimetry* (2011), pp. 113–122, [10.1142/9789814324922_0014](https://doi.org/10.1142/9789814324922_0014).
- [154] T. O. Niinikoski, *The Physics of Polarized Targets* (Cambridge University Press, Cambridge, England, 2020).
- [155] G. Reicherz, Status of polarized solid targets in European high energy scattering experiments, in *Talk given at the 24th International Spin Symposium* (2021), <https://indico2.riken.jp/event/3082/contributions/17424/attachments/10604/15030/Status-Compass-A2-CB-Elsa.pptx>.
- [156] I. Fernando, SpinQuest polarized target: An overview, in *Talk given at the 24th International Spin Symposium* (2021), https://indico2.riken.jp/event/3082/contributions/17319/attachments/10729/15238/SPIN2021_PolarizedTarget_IsharaFernando.pdf.
- [157] C. Keith, Testing a new polarized target for CLAS12 at Jefferson Lab, in *Talk given at the 24th International Spin Symposium* (2021), https://indico2.riken.jp/event/3082/contributions/17331/attachments/10704/15199/cketh_SPIN2021.pdf.
- [158] K. Ishizaki, ^{139}La polarized target study for NOPTREX, in *Talk given at the 2019 Workshop on Polarized Sources, Targets, and Polarimetry* (2019), <https://conference.sns.gov/event/139/contributions/250/attachments/308/1593/PSTP2019.pdf>.
- [159] C. D. Keith, J. Brock, C. Carlin, S. A. Comer, D. Kashy, J. McAndrew, D. G. Meekins, E. Pasyuk, J. J. Pierce, and M. L. Seely, The Jefferson Lab frozen spin target, *Nucl. Instrum. Methods Phys. Res., Sect. A* **684**, 27 (2012).

- [160] R. H. Dicke, The measurement of thermal radiation at microwave frequencies, in *Classics in Radio Astronomy* (Springer, New York, 1946), pp. 106–113.
- [161] A. Berlin, R. T. D’Agnolo, S. A. R. Ellis, C. Nantista, J. Neilson, P. Schuster, S. Tantawi, N. Toro, and K. Zhou, Axion dark matter detection by superconducting resonant frequency conversion, *J. High Energy Phys.* **07** (2020) 088.
- [162] R. Balkin, J. Serra, K. Springmann, S. Stelzl, and A. Weiler, White dwarfs as a probe of light QCD axions, [arXiv:2211.02661](https://arxiv.org/abs/2211.02661).
- [163] C. Ligi *et al.* (CUORE Collaboration), The CUORE cryostat: A 1-ton scale setup for bolometric detectors, *J. Low Temp. Phys.* **184**, 590 (2016).
- [164] C. Alduino *et al.*, The CUORE cryostat: An infrastructure for rare event searches at millikelvin temperatures, *Cryogenics* **102**, 9 (2019).
- [165] M. I. Hollister, R. C. Dhuley, and G. L. Tatkowski, A large millikelvin platform at Fermilab for quantum computing applications, *IOP Conf. Ser. Mater. Sci. Eng.* **1241**, 012045 (2022).
- [166] P. Astone *et al.*, First cooling below 0.1 K of the new gravitational-wave antenna “Nautilus” of the Rome group, *Europhys. Lett.* **16**, 231 (1991).
- [167] M. Cerdonio *et al.*, The ultracryogenic gravitational-wave detector AURIGA, *Classical Quantum Gravity* **14**, 1491 (1997).
- [168] M. G. Boulay (DEAP Collaboration), DEAP-3600 dark matter search at SNOLAB, *J. Phys. Conf. Ser.* **375**, 012027 (2012).
- [169] E. Aprile *et al.* (XENON Collaboration), Projected WIMP sensitivity of the XENONnT dark matter experiment, *J. Cosmol. Astropart. Phys.* **11** (2020) 031.
- [170] L. Di Luzio, B. Gavela, P. Quilez, and A. Ringwald, An even lighter QCD axion, *J. High Energy Phys.* **05** (2021) 184.
- [171] L. Di Luzio, B. Gavela, P. Quilez, and A. Ringwald, Dark matter from an even lighter QCD axion: Trapped misalignment, *J. Cosmol. Astropart. Phys.* **10** (2021) 001.
- [172] N. Crisosto, P. Sikivie, N. S. Sullivan, D. B. Tanner, J. Yang, and G. Rybka, ADMX SLIC: Results from a Superconducting LC Circuit Investigating Cold Axions, *Phys. Rev. Lett.* **124**, 241101 (2020).
- [173] L. Brouwer *et al.* (DMRadio Collaboration), DMRadio-m³: A search for the QCD axion below 1 μeV , *Phys. Rev. D* **106**, 103008 (2022).
- [174] C. Gatti and S. Tocci, FLASH: A proposal for a 100–300 MHz haloscope, in *Talk given at the Workshop on Physics Opportunities at 100–500 MHz Haloscopes* (2022), <https://indico.cern.ch/event/1115163/contributions/4685952/attachments/2393240/4091553/FLASH-100MHZ-HaloscopeWorkshop.pdf>.
- [175] A. Díaz-Morcillo, RADES at babyIAXO in the 400 MHz frequency range, in *Talk given at the Workshop on Physics Opportunities at 100–500 MHz Haloscopes* (2022), https://indico.cern.ch/event/1115163/contributions/4686032/attachments/2394076/4093137/RADES%20cavity-%20for%20BabyIAXO_def.pdf.
- [176] M. A. Hassan, Dielectric-loaded cavities for ADMX low-frequency searches, in *Talk given at the APS April Meeting* (2022), <https://meetings.aps.org/Meeting/APR22/Session/X07.3>.
- [177] P. Sikivie, N. Sullivan, and D. B. Tanner, Proposal for Axion Dark Matter Detection Using an LC Circuit, *Phys. Rev. Lett.* **112**, 131301 (2014).
- [178] S. Chaudhuri, P. W. Graham, K. Irwin, J. Mardon, S. Rajendran, and Y. Zhao, Radio for hidden-photon dark matter detection, *Phys. Rev. D* **92**, 075012 (2015).
- [179] Y. Kahn, B. R. Safdi, and J. Thaler, Broadband and Resonant Approaches to Axion Dark Matter Detection, *Phys. Rev. Lett.* **117**, 141801 (2016).